

EVOLUTION OF A MEMS PHOTOACOUSTIC CHEMICAL SENSOR

Paul M. Pellegrino and Ronald G. Polcawich

U.S. Army Research Laboratory, 2800 Powder Mill Road, Adelphi, MD 20783

ABSTRACT

Photoacoustic spectroscopy is a useful monitoring technique that is well suited for trace gas detection. The technique also possesses favorable detection characteristics when the system dimensions are scaled to a micro-system design. The objective of present work is to incorporate two strengths of the Army Research Laboratory (ARL), piezoelectric microelectromechanical systems (MEMS) and chemical and biological sensing into a monolithic MEMS photoacoustic trace gas sensor. A miniaturized macro-cell design was studied as a means to examine performance and design issues as the photoacoustics is scaled to a dimension approaching the MEMS level. Initial MEMS work is centered on fabrication of a lead zirconate titanate (PZT) microphone subsystem to be incorporated in the full photoacoustic device. Preliminary results were very positive for the macro-photoacoustic cell, PZT membrane microphones design / fabrication and elementary monolithic MEMS photoacoustic cavity.

INTRODUCTION

Photothermal spectroscopy encompasses a group of highly sensitive methods that can be used to detect trace levels of gases using optical absorption and subsequent thermal perturbations of the gases. The underlying principle that connects these various spectroscopic methods is the measurement of changes in physical parameters (temperature, pressure, or density) as a result of photo-induced change in the thermal state of the sample. Several examples of these techniques include photothermal interferometry (PTI), photothermal lensing (PTL), photothermal deflection (PTD), and photoacoustic spectroscopy (PAS). In PAS the pressure wave produced by the sample heating is measured, while the other techniques either measure changes in the refractive index or the refractive index directly by using combinations of probe sources and detectors. The photothermal method we have chosen to pursue is photoacoustic spectroscopy. Recent research suggests that trace gas detection at parts-per-trillion (ppt) levels are attainable with this particular photothermal technique.^{1,2} Although these studies demonstrate that photoacoustic sensors can meet the sensitivity requirements, the total system size would represent a large logistics burden in terms of size, cost, and power consumption.

Limited research has been done to demonstrate the feasibility of miniaturization of a PAS sensor to date.³⁻⁵ Initial examination of the scaling principles associated with PAS in respect to MEMS dimensions indicate the photoacoustic signals would remain at similar or surpass sensitivities commonly found in macro-scale devices.^{3,4} Several other issues including: increased stability, noise avoidance, small source-to-detector distances and monolithic sensor construction support the idea that a MEMS photoacoustic chemical sensor can be realized. The objective of the present work is to incorporate two

Report Documentation Page				Form Approved OMB No. 0704-0188	
Public reporting burden for the collection of information is estimated to average 1 hour per response, including the time for reviewing instructions, searching existing data sources, gathering and maintaining the data needed, and completing and reviewing the collection of information. Send comments regarding this burden estimate or any other aspect of this collection of information, including suggestions for reducing this burden, to Washington Headquarters Services, Directorate for Information Operations and Reports, 1215 Jefferson Davis Highway, Suite 1204, Arlington VA 22202-4302. Respondents should be aware that notwithstanding any other provision of law, no person shall be subject to a penalty for failing to comply with a collection of information if it does not display a currently valid OMB control number.					
1. REPORT DATE 01 JUL 2003		2. REPORT TYPE N/A		3. DATES COVERED -	
4. TITLE AND SUBTITLE Evolution Of A Mems Photoacoustic Chemical Sensor				5a. CONTRACT NUMBER	
				5b. GRANT NUMBER	
				5c. PROGRAM ELEMENT NUMBER	
6. AUTHOR(S)				5d. PROJECT NUMBER	
				5e. TASK NUMBER	
				5f. WORK UNIT NUMBER	
7. PERFORMING ORGANIZATION NAME(S) AND ADDRESS(ES) U.S. Army Research Laboratory, 2800 Powder Mill Road, Adelphi, MD 20783				8. PERFORMING ORGANIZATION REPORT NUMBER	
9. SPONSORING/MONITORING AGENCY NAME(S) AND ADDRESS(ES)				10. SPONSOR/MONITOR'S ACRONYM(S)	
				11. SPONSOR/MONITOR'S REPORT NUMBER(S)	
12. DISTRIBUTION/AVAILABILITY STATEMENT Approved for public release, distribution unlimited					
13. SUPPLEMENTARY NOTES See also ADM001523., The original document contains color images.					
14. ABSTRACT					
15. SUBJECT TERMS					
16. SECURITY CLASSIFICATION OF:			17. LIMITATION OF ABSTRACT UU	18. NUMBER OF PAGES 8	19a. NAME OF RESPONSIBLE PERSON
a. REPORT unclassified	b. ABSTRACT unclassified	c. THIS PAGE unclassified			

strengths of the ARL, piezoelectric MEMS and environmental sensing into trace gas sensor platform that addresses the problem of excessive logistical burden.

MACRO-CELL FABRICATION

The basic design for the macro-photoacoustic resonance cell (PRC) originated in the investigation conducted by Bijen *et.al.*² Our macro PRC design is a 1/4 scale down from the model cell studied by Bijen , with radius, $r_{\text{res}} = 0.75$ mm, and length, $l_{\text{res}} = 30$ mm (see Figure 1a). This unique cell design incorporates three strong noise suppressant characteristics: ZnSe Brewster windows, acoustic buffer volumes and tunable air columns. A Brewster's window, in an appropriate material for the wavelength of interest, has been shown to be a superior entrance window for the excitation light, providing low losses and minimal absorption thereby reducing thermal signatures from the entrance window. The acoustic buffer volumes with proper dimensions, $r_{\text{buf}} \sim 3r_{\text{res}}$ and $l_{\text{buf}} \sim l_{\text{res}}/2$, provide for decoupling of the open tube resonator from the surrounding buffer volume ensuring the resonator is acoustically isolated. The last suppression mechanism built into the macro-cell involves tunable air columns that can be positioned to provide constructive interference with noise signals originating from the window of the cell. Several other considerations involving the focusing parameters of the light were taken into account to reduce any stray absorption associated with surface interactions. The optimal focusing of the excitation beam is constrained by requirements that the confocal parameter equals the acoustical resonator length (l_{res}) and the beam radius equals 1/3 the acoustic resonator radius (r_{res}). Imposing these constraints on the excitation beam focusing ensured clear aperture and quasi-collimation through the acoustic buffer and resonator regions. Figure 1b displays the fabricated macro-PRC.

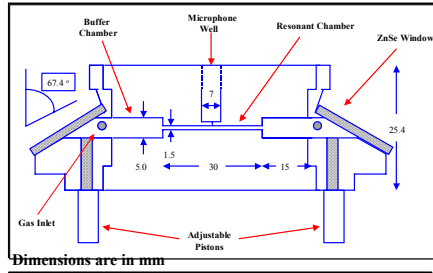


Figure 1. a) Mechanical drawing of macro-PRC b) Photograph of the fabricated macro-PRC.

MICROPHONE FABRICATION

A piezoelectric microphone based on PZT thin films was designed in order to investigate its potential use as a passive sensing element in a PRC. The microphone fabrication process began with a double side polished silicon wafer and utilized several different types of deposition systems. A plasma enhanced chemical vapor deposited (PECVD) silicon dioxide thin film was deposited with a Plasma-Therm 790 reactor using a mixture of SiH_4 , He, and N_2O . The oxide served as the membrane structural layer and was chosen to be between 1 – 2 μm thick depending on the final PZT thickness chosen. After deposition, the film was annealed in an A.G. Associates Heatpulse 610 rapid thermal anneal (RTA) furnace at 700°C for 60 seconds in flowing nitrogen. This anneal removes the trapped hydrogen within the film and causes the film to obtain a slightly tensile stress, which increases the performance of the final membrane structure.

After the oxide is deposited and annealed, a metal electrode was sputter deposited to serve both as the bottom electrode and as a growth template for the piezoelectric actuator. For adhesion to the oxide, a thin layer (200 Å) of titanium was first sputtered and was immediately followed by the platinum deposition (800 Å) without breaking vacuum within a Varian 3190 DC magnetron sputter deposition

system. Following the platinum deposition, the wafers were annealed in the RTA furnace at 700°C for 60 seconds in flowing dry air in order to improve the adhesion between the oxide and metal layers and the surface texture of the platinum prior to deposition of the piezoelectric thin film. The next fabrication step was to deposit the lead zirconate titanate (PZT) thin film. The deposition process is a solution spin on process. First, a PZT sol-gel solution was prepared following a modified alkoxide process first introduced by Budd, Dey, and Payne.⁶ This process used lead acetate trihydrate, zirconium n-propoxide, and titanium isopropoxide as the precursors and 2-methoxyethanol as the solvent. Once the sol-gel solution has been prepared and aged, the repetitive deposition process began with a portion of the sol dispensed onto a platinized silicon substrate. The wafer was then spun at 2500 rpm for 30 seconds. Next, the wafers were placed onto a hotplate at 350°C for 120 seconds, which causes the film to undergo pyrolysis thereby decomposing all the organics. This process of deposition, spin, and pyrolysis was then repeated a total of 4 times. After the last pyrolysis, the wafer was annealed in a RTA furnace at 700°C for 30 seconds in flowing air in order to crystallize the PZT thin film. The result was approximately a 0.25 μm PZT film and the process is continued in order to achieve the desired thickness of a 1 μm PZT thin film.

After the piezoelectric was deposited, a top electrode of platinum (800 Å) was sputter deposited onto the wafer surface. The wafers were then annealed in a RTA at 350°C for 120 seconds in flowing air to improve adhesion and reduce any sputtering induced surface damage. The resultant wafer stack at this stage is Si/SiO₂/Ti/Pt/PZT/Pt. The first step in the microphone fabrication is to define the final actuator dimensions and the location of the electrical contacts. Because electrical contact has to be made to the bottom Ti/Pt electrode, a sacrificial titanium layer was electron beam evaporated onto the wafer and patterned with a liftoff technique. The next step was to pattern the wafer with AZ 5214E positive photoresist. To define the final actuator dimensions, argon ion-milling was employed to sputter remove the Ti/Pt/PZT/Pt stack from a majority of the wafer. During this process, the sacrificial Ti layer will prevent the ion-milling of approximately half the PZT layer and all of the Ti/Pt bottom electrode.

After removal of the photoresist, another resist pattern was placed onto the wafer in order to open windows to the bottom electrode. Within these windows the structure was Si/SiO₂/Ti/Pt/PZT. The PZT was then wet etched using H₂O:HCl:HF (2:1:0.02) in order to expose the Pt. Afterwards, the photoresist was removed with photoresist stripper at 85°C. The next step in the fabrication was to deposit a 2500 Å PECVD SiO₂ thin film that will serve as an isolation layer preventing electrical contact between the top and bottom electrical traces. After deposition, the film was annealed in a RTA at 350°C for 120 seconds in flowing N₂ and then again for 120 seconds in flowing air. This anneal improves the adhesion between the structural silicon dioxide that was first deposited and the isolation oxide. The next step was to pattern the oxide around the circumference of the actuator. Again positive photoresist was used and the wafer was placed into a LAM 590 etch system in which the oxide was etched using a CHF₃/CF₄ plasma.

To make electrical contact to the top Pt electrode of the actuator, an evaporated 200 Å Ti / 2500 Å Au layer was deposited and patterned with a liftoff technique. The Ti/Au was also deposited onto the bottom Ti/Pt electrode so that gold wire bonding could be used to package the final devices. The last step in the fabrication was a deep reactive ion etch (DRIE) of the silicon substrate in order to release the membrane actuator. Using a Karl-Suss MA/BA 6 mask aligner, a 6 μm thick positive photoresist (AZ 9245) was patterned onto the reverse side of the silicon substrate. The silicon DRIE was performed using a Unaxis VLR clustertool configured with an inductively coupled plasma (ICP) etch chamber. The process followed the Bosch⁷ process using a cyclical etch process consisting of a polymer deposition with a C₄F₈ plasma followed by an isotropic silicon etch with a SF₆ plasma. After etching, the remaining photoresist was removed with an oxygen plasma. The complete membrane devices were separated into die using scribe lines that were etched during the Si DRIE step. The separated device die was subsequently packaged using a TO-8 package that was predrilled with a circular release hole. The release

hole allows the membrane to deflect and freely push air out the opening, thereby reducing the deleterious effect of squeeze film damping.

ACOUSTIC TESTING

Initial exploration of the open tube resonance of the macro-cell was investigated by flooding the cell with amplified white noise. The broadband white noise (0-100kHz) was generated using an ACO Pacific, Inc. generator that was amplified using a McIntosh tube-based amplifier. This white noise was introduced into the macro-cell via Tygon[®] tubing through the gas inlet after the tube was split to allow a portion of the white noise to be diverted to a reference Brüel & Kjær (B&K) microphone. These initial attempts failed to produce a reliable resonance signal in the macro-cell cavity. Our inability to drive the cell's resonance could stem from several possible factors including: acoustical impedances from the tubing and gas fixtures and the buffer volume itself decoupling the resonator from it's surrounding as it was designed to do. The failure of the resonance explorations using the tube-generated white noise prompted investigations of the resonance structures by driving the macro-cell with amplified white noise projected by speakers inside an anechoic chamber containing the macro-cell without window assemblies.

Evaluating the performance of a PZT microphone was accomplished by placing a packaged microphone die into an electrical test chamber (as seen in Figure 2) with rubber grommet seals to prevent outside noise interference. An acrylic cap was placed atop the packaged microphone die and a Tygon[®] tube was attached between the acrylic cap and the tube driver assembly. The acoustic test chamber was configured with BNC mounts for electrical connection and a 1/8" ID nozzle for connecting to the Tygon[®] tube from the tube driver.

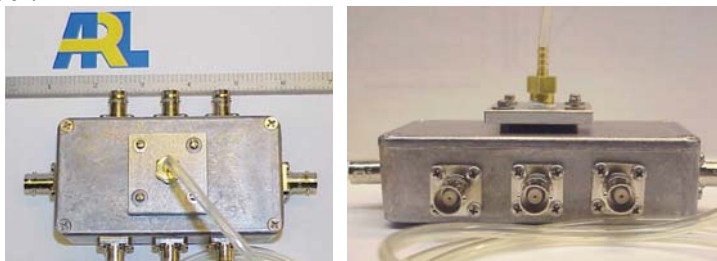


Figure 2. Images of the acoustic test chamber used for testing the PZT microphone.

The tube driver was driven with either a 1 kHz pulse or white noise with a gain of -10 dB. The generated acoustic wave was picked up by both a B&K calibrated microphone and the PZT microphone. The data was collected with Labview software and subsequently analyzed using a Matlab algorithm. In addition to the tube driver experiments, the acrylic cap could be removed and a NIST calibrated tone source of 64 or 94 dB could be placed atop the PZT microphone package. The same source could then be connected to the B&K microphone and a direct comparison between the two microphones could occur.

PHOTOTACOUSTIC TESTING

The principal behind photoacoustic sensing is conversion of photonic energy to acoustic energy by exciting an analyte of interest with a light source tuned to a molecular absorption of the analyte. In particular, the system used in this research is described as a resonant photoacoustic technique. This system incorporates a known acoustic resonance structure into the photoacoustic cell and the corresponding modulation to the light source to oscillate and store the acoustic energy. This architecture can enhance the sensitivity of the sensor 1-2 orders of magnitude over non-resonance cell configurations. The basic photoacoustic system involves: a modulated light source, chopper, spectrum analyzer, acoustic cell, power meter, and lock-in amplifier.

Investigations involving the fabricated macro-cell were performed on a test-bed diagramed in Figure 3. The Laser Photonics model CL55 waveguide CO₂ laser was tuned to the P(18) rotation line at approximately 10.58 μm in wavelength. This wavelength corresponds well to an absorption line of the trace gas studied (SF₆). The power output on this laser line was typically 6 Watts of continuous wave power with a drift of less than 0.5%. The beam was immediately passed through a New Focus model 3501 optical chopper (50% duty cycle) that could provide modulation from 4-6400 Hz. The beam was split (50/50) into two components, one corresponding to a spectral measurement and the other used to drive the photoacoustic resonance cell. The spectral measurement was recorded using a Macken Instruments model 16A CO₂ spectrum analyzer. The excitation beam was focused through the macro-cell using a $f = 63.5$ mm lens producing a measured beam diameter of 450 μm at $1/e^2$ intensity. The modulated acoustic signal was detected with a Knowles model 3524 amplified electret microphone, which input directly into a Stanford Research Systems model SR510 lock-in amplifier. The transmitted laser power was measured with a Ophir Nova power meter equipped with a model 30A thermal head. These power measurements provided a scale term to normalize the photoacoustic signal for any residual drift associated with the excitation source. The trace gas used in these studies, SF₆, was generated using a permeation tube device manufactured by VICI Metronics, Dynacalibrator model 190. The SF₆ source was a certified wafer device placed into the permeation oven held at a constant temperature of 40°C and exposed to calibrated flows of 200-800 mL/min. Larger flow rates were not used due to onset of turbulent flow, which dramatically increased the noise floor of the microphone used even with lock-in amplification.

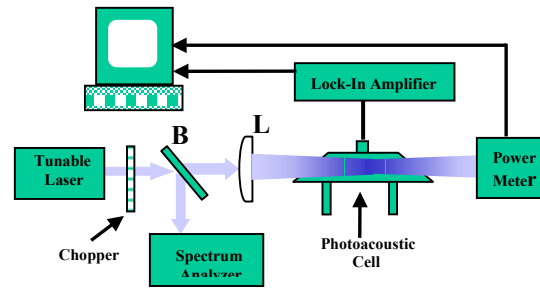


Figure 3. Schematic of general photoacoustic measurement system.

The acoustic testing on the macro-cell underwent to distinct realizations. As stated earlier, the initial tests involving the tube driver could not consistently produce a resonance response in the macro-PRC open-tube resonator. More extensive investigations were performed in the anechoic chamber with the results being displayed in Figure 4a. There seems to be two resonance peaks present under 10 kHz. The fundamental mode corresponding to the $v_{res} = c / 2l_{res}$ relationship should have appeared at approximately 5.5 kHz for a $l_{res} = 30\text{mm}$. The resonance peak appearing at 4.7 kHz corresponds well with the fundamental mode when shifting of the resonance frequency due to the buffer volumes and the microphone channel are taken into account. The energy storage ability of the mode, the quality factor (Q), was measured to be $Q \sim 50-60$ for the fundamental mode agreeing with calculated values based on the dimensions of the present cavity structure. The appearance of a second mode around 7.2 KHz was not anticipated and does not correspond well with fundamental resonant modes of the open tube resonator design. This mode may be a combination mode involving several overtone of the resonator and will require modeling studies to discern its origins.

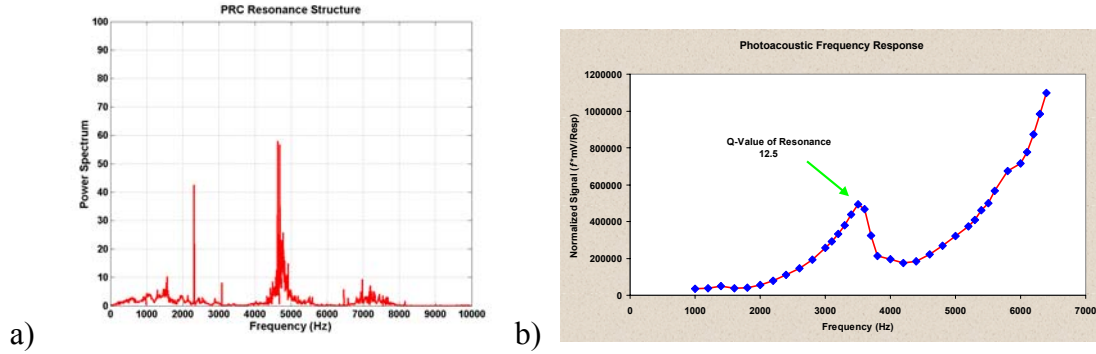


Figure 4. a) Resonance structure of the macro-PRC without Brewster's window assemblies.
b) Resonance structure of macro-PRC probed by photoacoustic sensing.

Although this analysis performed as expected, we were unable to discern resonance structure under the conditions that the cell would be operated. Once the Brewster's window assemblies are attached to the macro-cell body and seal the resonator, the frequency of the fundamental modes in the open tube resonator are expected to shift due to the newly imposed hard boundary conditions of these assemblies. The first photoacoustics experiments performed incorporating the sealed PRC in the optical train were centered on determining on frequency response. Figure 4b shows the typical frequency response of the fully sealed PRC when exposed to constant SF_6 gas concentration. The data has been scaled to remove the typical $1/f$ bias and the microphone response in order to give a representative look of the response of the PRC. The expected shifting of the resonance modes has occurred with the fundamental appearing at approximately 3.4 kHz and the second undetermined mode appearing at the end of our modulation ability (6.4 kHz). Other important features exhibited in the PRC response is the Q associated with the fundamental mode ($Q \sim 12.5$) and the accentuation of the second mode. Initially the appearance of the second mode could not be assigned to the excitation of the $\nu = l_{\text{res}}$ harmonic, but examination of the sealed PRC has accentuated the response of this harmonic and shifted the resonance to a frequency that corresponds well with a harmonic of the fundamental at 3.4 kHz. Again a full modeling of the acoustic cavity will be required to de-convolute the resonance structure in the presence of complex boundary conditions.

Tests on the sensitivity of the PRC were conducted both off and on resonance. These tests were conducted to investigate the linearity, dynamic range, relative and calibrated sensitivities. Figure 5a shows the off-resonance photoacoustic signal response of the PRC flooded with varying N_2/SF_6 mixtures. The off-resonance test conducted at 1792 Hz demonstrated large signals (~ 0.2 - 1.0 mV/W) for SF_6 concentrations ranging from 250-1000 ppb. The response exhibited good linearity with a correlation coefficient of $R^2 = 0.978$. The overall signal-to-noise (S/N) values in the off-resonance conditions were astonishingly high ($\sim 400:1$). Figure 5b shows the on-resonance response of the PRC flooded with identical N_2/SF_6 gas concentrations. The on-resonance tests were conducted at 3420 Hz maximizing the signal response from the PRC tube resonator. The signal levels were extremely large in magnitude (~ 2 - 10 mV/W) and in relation to the noise floor ($\text{S/N} \sim 4200:1$). The linearity of the on-resonance signals were superior to the off-resonance signals demonstrating an excellent correlation coefficient of $R^2 = 0.998$. The relative signals strength of the on versus off resonance conditions reaffirms that the energy storage capability of the PRC or its Q is approximately 10 X. Using the S/N associated with the measurement at the lowest concentration demonstrated in this study (270 ppb), a projected LOD for SF_6 vapor is estimated at 65 ppt. The sensitivity of this measurement in absolute terms corresponds to an absorbance of $2.2 \times 10^{-8} \text{ cm}^{-1}/\text{W}$, which is well above theoretically projected limits, but only an order of magnitude above demonstrated research grade photoacoustic instruments.

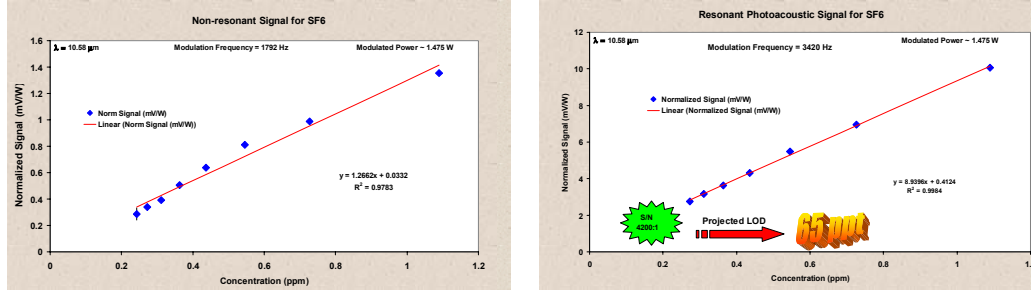


Figure 5. PRC a) non-resonant and b) resonant response for varying concentrations of SF_6 vapor.

The Q of the open tube resonator used in the PRC was estimated in both the frequency response and the off-on resonance comparisons to be approximately 12.5. When this Q is compared to the published Q for the resonator that this design was modeled after, the value has been reduced by a factor of approximately 2.4. The scaling of this parameter should follow the proportionality $Q \propto r_{\text{res}}/(l_{\text{res}})^{1/2}$, which would indicate a reduction in the value when the cell is scaled downward. Inputting the appropriate figures into the Q proportionality equation indicates the Q seen with our resonator should be reduced by a factor of 2.2. These results indicate that the scaling law for this type of resonator structure holds to first approximation. This information could prove invaluable as a guide to design a MEMS-scale PRC that maintains a Q for the fundamental mode of the open tube resonator ensuring sensitivities analogous to its macro-PRC counterpart.

The first step in developing an integrated MEMS PRC was the fabrication of a piezoelectric MEMS microphone. The PZT membrane microphones were successfully fabricated and are displayed in Figure 6. The optical micrograph in Figure 6a illustrates that only 80% of the diaphragm diameter is covered by the piezoelectric. The PZT has been removed from the outer 20% to maximize the sensitivity by eliminating the conflicting strain response between the outer and inner portions of a deflecting membrane. The cross section SEM in Figure 6b shows the silicon DRIE release via used to create the suspended membrane.

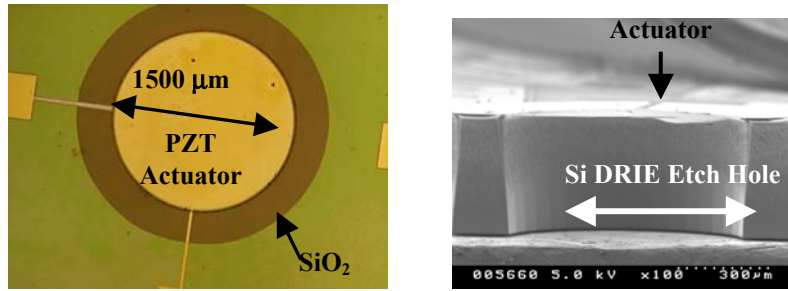


Figure 6: a) Micrograph of PZT membrane actuator b) SEM image of silicon DRIE release via.

Figure 7a provides a plot of the acoustic response from 3 different 1500 μm diameter microphones and the B&K calibrated microphone for an uncalibrated ~ 1 kHz tone. The PZT microphone performed quite well in these early experiments and clearly picked up the ~ 1 kHz tone. A majority of the noise in the PZT response has been attributed to bit noise during data acquisition and chamber losses during the measurement. To improve output signal from the PZT microphones, a Stanford Research Systems operational amplifier was added during the measurements. With a gain of 100 – 1000, the PZT signal began to approach that of the B&K (see Figure 7b) without significant loss in the signal to noise ratio. To determine the operational bandwidth of the PZT microphone, the microphones were subjected to white noise and data was collected up to 112.5 kHz. Examining the white noise output from the microphone indicated a flat band response up to 112.5 kHz, which was to be expected as the mechanical resonance of the microphone should be on the order of 125 - 150 kHz

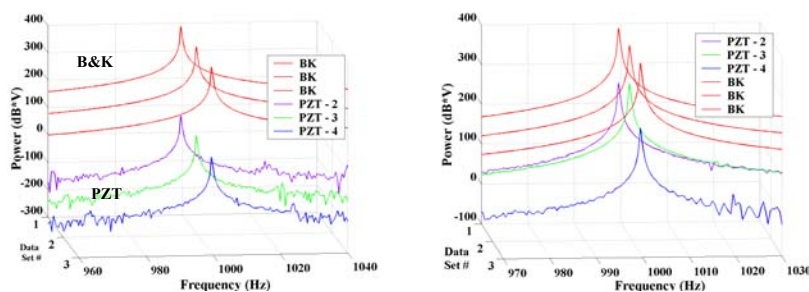


Figure 7: Acoustic response of a B&K and a 1500 μm diameter PZT MEMS microphone for an uncalibrated 1 kHz tone: (left) unamplified and (right) amplified with 1000 gain.

CONCLUSION

Our investigation resulted in the successful fabrication and testing of a macro-PRC that is 1/4 scale of previous published reports. This macro-PRC design demonstrated sensitivity of 270 ppb of SF_6 trace gas with a S/N of 4200:1, implying a projected LOD of 65pptr. Photoacoustic testing of the macro-PRC concluded that miniaturization of a PAS system is viable without a significant loss in signal. No adverse effects of the size scaling were visualized in the optics or acoustics of the macro-PRC. Additionally, the scaling law for the Q of longitudinal resonant structure was proven to be valid in a scaled macro-PRC. Proper engineering of the appropriate dimensions could allow for the design of a MEMS PRC that is equally as sensitive as its macroscopic counterparts.

Initial MEMS research successfully fabricated a piezoelectric microphone for acoustic sensing. The PZT microphones were shown to perform well up to their mechanical resonant frequency and may provide a low power means of detecting PAS signals. The microphones were further miniaturized to correspond to the MEMS PRC requirements. Electromechanical evaluation of the smaller microphones has shown that they still exhibit good performance up their fundamental resonant frequency.

REFERENCES

1. M. Nägele, M.W. Sigrist, "Mobile laser spectrometer with novel resonant multipass photoacoustic cell for trace-gas sensing," *Appl. Phys. B* **70**, pp. 895-901 (2001).
2. F.G.C. Bijnen, J. Reuss, and F.J.M. Harren, "Geometrical optimization of a longitudinal photoacoustic cell for a sensitive and fast trace gas detection," *Rev. Sci. Instrum.* **67**, pp. 2914-2933 (1996).
3. S.L. Firebaugh, K.F. Jensen, and M.A. Schmidt, "Miniaturization and Integration of Photoacoustic Detection with a Microfabricated Chemical Reactor System," *JMEMS*, **10**, pp 232-237, (2001).
4. S.L. Firebaugh, K.F. Jensen, and M.A. Schmidt, "Miniaturization and integration of photoacoustic detection," *J. Appl. Phys.* **92**, pp.1555-1563 (2002).
5. U. Bonne, B.E. Cole, and R.E. Higashi, US Patent No. 5,886,249.
6. K.D. Budd, S.K. Dey, D.A. Payne, "Sol-Gel Processing of PbTiO_3 , PbZrO_3 , PZT, and PLZT Thin Films," *Brit. Cer. Proc.*, **36**, pp. 107-21 (1985).
7. F. Laermer and A. Schilp, "Method of Anisotropically Etching Silicon", US-Patent No. 55018893.